

Efficient Speech Command Recognition Leveraging Spiking Neural Network and Curriculum Learning-based Knowledge Distillation

Jiaqi Wang^{1,2}, Liutao Yu², Liwei Huang^{2,3}, Chenlin Zhou², Han Zhang^{2,4}, Zhenxi Song¹, Min Zhang¹, Zhengyu Ma^{2*}, Zhiguo Zhang^{1,2†}

¹Harbin Institute of Technology Shenzhen, ²Peng Cheng Laboratory, ³Peking University, ⁴Harbin Institute of Technology

Abstract

The intrinsic dynamics and event-driven nature of spiking neural networks (SNNs) make them excel in processing temporal information by naturally utilizing embedded time sequences as time steps. Recent studies adopting this approach have demonstrated SNNs' effectiveness in speech command recognition, achieving high performance by employing large time steps for long time sequences. However, the large time steps lead to increased deployment burdens for edge computing applications. Thus, it is important to balance high performance and low energy consumption when detecting temporal patterns in edge devices. Our solution comprises two key components. 1). We propose a high-performance fully spike-driven framework termed SpikeSCR, characterized by a global-local hybrid structure for efficient representation learning, which exhibits long-term learning capabilities with extended time steps. 2). To further fully embrace low energy consumption, we propose an effective knowledge distillation method based on curriculum learning (KDCL), where valuable representations learned from the easy curriculum are progressively transferred to the hard curriculum with minor loss, striking a trade-off between power efficiency and high performance. We evaluate our method on three benchmark datasets: the Spiking Heidelberg Dataset (SHD), the Spiking Speech Commands (SSC), and the Google Speech Commands (GSC) V2. Our experimental results demonstrate that SpikeSCR outperforms current state-of-the-art (SOTA) methods across these three datasets with the same time steps. Furthermore, by executing KDCL, we reduce the number of time steps by 60% and decrease energy consumption by 54.8% while maintaining comparable performance to recent SOTA results. Therefore, this work offers valuable insights for tackling temporal processing challenges with long time sequences in edge neuromorphic computing systems.

Introduction

Recognized as the third generation of neural networks (Maass 1997), spiking neural networks (SNNs) effectively mimic the dynamics of biological neurons with sparse and asynchronous spikes. This approach enables SNNs to achieve high computational performance with low energy consumption, making them a viable energy-efficient alternative to artificial neural networks (ANNs) (Fang et al. 2023).

Recent studies (Kugele et al. 2020; Yao et al. 2021; Kim et al. 2023; Zhu et al. 2024) have demonstrated that the spiking mechanisms of SNNs excel in handling temporal data and event-driven applications, capitalizing on their inherent spatio-temporal encoding capabilities. These unique capabilities make SNNs exceptionally well-suited for processing constantly evolving dynamic content, such as speech and audio. While ANNs have demonstrated effectiveness in handling various acoustic features like Mel-frequency cepstrum coefficients (Logan et al. 2000), Mel spectrograms (Shen et al. 2018), and other audio representations in speech recognition tasks, their inherent architecture inevitably leads to high energy consumption (Yang et al. 2022). This poses a non-negligible obstacle when deploying ANNs in speech command recognition (SCR) in energy-restricted scenarios, such as mobile and wearable devices, where both high accuracy and low energy consumption are crucial. In response, the natural temporal dynamics and event-driven property inherent in SNNs not only align with the properties of audio but also cater to the urgent needs for efficiency and effectiveness in speech processing systems, offering a promising solution for developing energy-efficient neuromorphic technologies (Xu et al. 2023a).

Since the inherent capabilities of SNNs align well with the requirements of SCR, an SNN-based model is essential to fully exploit these strengths. However, two critical challenges remain in developing such a high-performance and energy-efficient model for SCR. First, the efficient learning of contextual information across multi-level remains largely unexplored. While local context captures fine-grained details, it lacks an overall perspective, which will hinder the understanding of the command's intent and increase sensitivity to noise. Conversely, global context provides a broader understanding but may miss essential details needed to differentiate similar commands. Second, achieving a balance between high performance and energy efficiency has been largely overlooked. Recent SNN studies (Bittar and Garner 2022; Hammouamri, Khalfaoui-Hassani, and Masquelier 2024; Deckers et al. 2024) have leveraged the embedded time sequences as time steps. This approach aligns well with the dynamics of SNNs, as it avoids artificially increasing dimensions through repetition. However, directly using these time sequences can lead to higher accuracy but also increases the energy burden. A potential solution involves

*Corresponding author

†Corresponding author

downsampling the time sequences to create shorter time steps (Wu et al. 2023; Liu et al. 2024a), but this solution can compromise performance.

To address the aforementioned challenges in leveraging SNNs for SCR, our solution focuses on both enhancing the performance of SNNs and optimizing energy efficiency. Specifically, we introduce SpikeSCR, an innovative fully spike-driven framework. It is designed to capture both global and local contextual information within input sequences, thereby providing a fine-grained and comprehensive understanding. In terms of global representation learning, SpikeSCR develops a refined spike-driven attention mechanism, which builds on the spiking self attention (SSA) (Zhou et al. 2023) by integrating rotary position encoding (RoPE) (Su et al. 2024), leveraging the importance of positional information in temporal dynamics to improve contextual learning. In terms of local representation learning, we propose a separable convolutional module equipped with a gated mechanism (Gulati et al. 2020), which efficiently captures critical dependencies by selectively controlling information flow, maintaining sparse computation and boosting performance with minimal resource usage.

Further, to address the high energy consumption issues associated with long time steps, we introduce a knowledge distillation method based on curriculum learning, termed KDCL. In KDCL, learning processes using long time steps are designated as easy curricula, whereas those involving shorter time steps are considered harder curricula. KDCL can efficiently and progressively transfer the valuable knowledge from models trained on longer time steps to those using shorter time steps with minor information loss, thus reducing energy consumption and maintaining performance levels comparable to SOTAs. This KDCL method has significant potential for improving performance in edge computation scenarios with limited time steps.

Our main contributions are summarized below:

- We propose SpikeSCR, a fully spike-driven SNN framework with a global-local hybrid architecture for efficient representation learning and exhibiting long-term learning capabilities with extended time steps.
- We introduce KDCL, an effective curriculum learning-based knowledge distillation method, progressively transferring valuable representations from easy to hard curriculum with minor loss, achieving a satisfactory trade-off between energy consumption and performance.
- Extensive experiment results on SHD, SSC, and GSC datasets exhibit that SpikeSCR surpasses SOTAs with the same time steps. Through KDCL, it maintains comparable performance while reducing time steps by 60% and energy consumption by 54.8%.

Related Works

Deep Spiking Neural Networks

There are primarily two major approaches to obtain a trained SNN. One is ANNs-to-SNN conversion (Deng and Gu 2021; Bu et al. 2022; Xu et al. 2023b), where a high-performance pre-trained ANN is transformed into an SNN by replacing

its ReLU activation layers with spiking neurons (Rathi and Roy 2021). While the converted SNNs can achieve excellent performance, they often require a long-term simulation with hundreds or even thousands of time steps to accurately approximate the ReLU activations, which leads to large latency (Su et al. 2023; Guo et al. 2024). The other is direct training, the application of backpropagation-through-time (BPTT) on SNNs enables end-to-end training from scratch (Nefci, Mostafa, and Zenke 2019). Notably, this approach involves using surrogate gradient functions to approximate the derivatives of the non-differentiable Heaviside step function, which is essential for the spiking mechanism (Lee, Delbruck, and Pfeiffer 2016; Lee et al. 2020). Recent impressive works (Sengupta et al. 2019; Fang et al. 2021; Zhou et al. 2023; Yao et al. 2024) have dedicated efforts to translating de-facto standard models from ANNs into new architectures that conform to the calculation characteristics of SNNs.

SNNs for Speech Command Recognition

Speech command recognition, also known as keyword spotting, demands accurate recognition and low energy consumption, and it is crucial for numerous edge computing applications (Warden 2018). Recent SNNs have demonstrated considerable promise in meeting these requirements. Several studies (Yang, Liu, and Li 2022; Dampfhofer et al. 2022) have concentrated on enhancing network architecture to achieve high accuracy and energy efficiency in low-resource settings. Notably, further developments (Hamouamri, Khalfaoui-Hassani, and Masquelier 2024; Sun et al. 2023b; Deckers et al. 2024) involve novel methods for learning delays in SNNs, addressing the critical challenge of plastic delays for the timing of spike arrivals. Additionally, recent works (Bittar and Garner 2022; Zhang et al. 2024b; Deckers et al. 2024) have proposed innovative spiking neurons for better learning dynamic time series. Moreover, substantial efforts (Stewart et al. 2023; Cramer et al. 2020) have been made to provide novel artificial cochleas models or spike generation pipelines, contributing to the advancement of neuromorphic speech recognition systems.

The aforementioned works often rely on long time sequences to approximate hundreds or more time steps, leading to a tendency towards higher energy consumption. The challenge of optimizing the balance between energy consumption and performance is unresolved. Resolving this challenge could significantly improve the efficiency and deployment of neuromorphic technologies in power-sensitive environments, enhancing both energy sustainability and the accessibility of speech processing applications.

Methods

Spiking Neuron

Spiking neurons are a crucial component of SNNs, which can serve as bio-plausible abstractions (Rathi et al. 2023). We adopt the Leaky Integrate-and-Fire (LIF) neuron, which has been widely proven effective (Roy, Jaiswal, and Panda 2019). The dynamics of a LIF neuron are described as:

$$H[t] = V[t - 1] + \frac{1}{\tau} (X[t] - (V[t - 1] - V_{reset})), \quad (1)$$

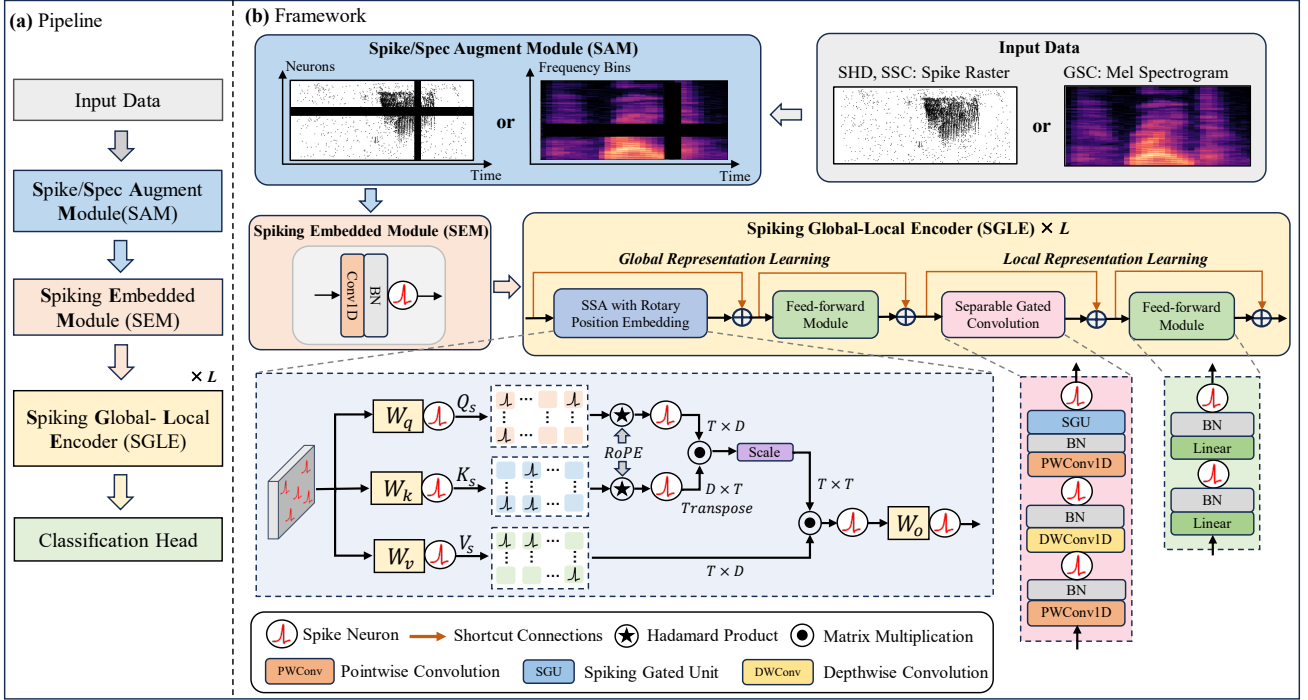


Figure 1: Method Overview: (a) The pipeline of SpikeSCR. (b) The framework of SpikeSCR consists of a spike/spec augment module (SAM), a spiking embedded module (SEM), spiking global-local encoders (SGLE) with L blocks, and a linear classification head. All the modules are spike-driven, consistent with SNN’s computational characteristics.

$$S[t] = \Theta(H[t] - V_{th}), \quad (2)$$

$$V[t] = H[t](1 - S[t]) + V_{reset}S[t], \quad (3)$$

where τ is the membrane time constant, $X[t]$ is the input current at time step t , V_{reset} is the reset potential, V_{th} is the firing threshold. Eq. (1) describes the update of membrane potential. Eq. (2) describes the spike generation process, where $\Theta(v)$ is the Heaviside step function: if $H[t] \geq V_{th}$ then $\Theta(v) = 1$, meaning a spike is generated; otherwise $\Theta(v) = 0$. $S[t]$ represents whether a neuron fires a spike at time step t . Eq. (3) describes the resetting process of membrane potential, where $H[t]$ and $V[t]$ represent the membrane potential before and after the evaluation of spike generation at time step t , respectively.

SpikeSCR Architecture

Spike/Spec Augment Module (SAM). As shown in Figure 1(b), we utilize the augmentation by SpecAugment (Park et al. 2019) with frequency mask and time mask for the Mel spectrogram of the input audio. For the spike trains, we utilize a method similar to EventDrop (Gu et al. 2021), which involves two operations: drop-by-time and drop-by-neuron, both performed at a fixed ratio to drop events in different dimensions randomly. Due to space constraints, the implementation details are provided in Appendix A.

Spiking Embedded Module (SEM). The SEM is structured by sequentially stacking $\{\text{Conv1D-BN-LIF}\}$. Given the input \mathbf{X} , the process of SEM can be formulated as,

$$\text{SEM}(\mathbf{X}) = \text{SN}(\text{BN}(\text{Conv}(\mathbf{X}))), \quad (4)$$

where SN is the spiking neuron. This structure confers several advantages. Firstly, the $\{\text{Conv1D-BN}\}$ ensures effective representation learning and sets up appropriate dimensions for the mechanism of multi-head attention computation in the subsequent SSA module. Secondly, the LIF neuron encodes the features into spike trains (Rathi and Roy 2021; Zhou et al. 2023; Shen et al. 2024) as a spike generator.

Spiking Global-Local Encoder (SGLE). Inspired by previous works (Vaswani et al. 2017; Gulati et al. 2020; Yao et al. 2024), we introduce a novel architecture termed SGLE, designed to effectively capture both broad global and detailed local features, as illustrated in Figure 1(b).

For global representation learning, we utilize the SSA mechanism to capture long-range dependencies. To incorporate positional information in temporal dynamics, we added RoPE into the SSA. Given the spike input \mathbf{X}_S , the internal mechanisms are described as follows,

$$Q_S = \text{SN}_Q(\mathbf{W}_Q(\mathbf{X}_S)), \quad K_S = \text{SN}_K(\mathbf{W}_K(\mathbf{X}_S)), \quad (5)$$

$$Q'_S = \text{SN}_{R_Q}(R_Q \odot Q_S), \quad K'_S = \text{SN}_{R_K}(R_K \odot K_S), \quad (6)$$

$$V_S = \text{SN}_V(\mathbf{W}_V(\mathbf{X}_S)), \quad (7)$$

$$\text{SSA}(Q'_S, K'_S, V_S) = \text{SN}((Q'_S K'^T_S V_S * s), \quad (8)$$

where SN is the spiking neuron, \mathbf{W} is the learnable weight matrix of $\{\text{Linear-BN}\}$, R is the rotary position matrix, \odot is the Hadamard Product, s denotes a scale factor to avoid the gradient vanishing caused by the large integers.

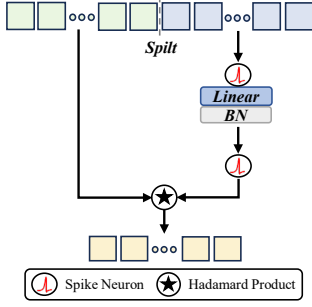


Figure 2: Spiking Gated Unit.

For local representation learning, we first propose a spiking gated unit (SGU) module to enhance the performance of lightweight Conv-assemblies, as shown in Figure 2. The SGU can be viewed as a spiking version of the Gated Linear Unit (Dauphin et al. 2017; Gulati et al. 2020), featuring a selective gating mechanism for information flow. It processes split feature embeddings X_1 and X_2 , described as follows:

$$SGU(X_1, X_2) = X_2 \odot (SN_2(W(SN_1(X_1))))), \quad (9)$$

where W is the learnable weight matrix of $\{\text{Linear-BN}\}$, \odot is the Hadamard Product. SN_1 aims to spikify the float-point inputs, SN_2 aims to regulate the transmission of information flow, and both are designed to implement sparse accumulate (AC) operations (Datta et al. 2022). We then summarize the proposed separable gated convolution (SGC) into three blocks, operating on the input X as follows:

$$SGC(X) = SN(P_{WG}(SN(D_W(SN(P_W(X)))))) \quad (10)$$

where P_W is the pointwise (PW) convolution, P_{WG} is the PW convolution with SGU, and D_W is the depthwise convolution with a kernel size of 31. BN operations are considered foldable weights inserted into the convolutional stems.

KDCL

Curriculum Learning. As illustrated in Figure 3, we propose an effective curriculum learning-based knowledge distillation method (KDCL) to optimize the trade-off between performance and energy consumption. We define the teacher model’s initial learning from longer time steps as the easy curriculum. This knowledge is progressively transferred to student models with shorter time steps, defined as the hard curriculum. The learning process of KDCL is thoroughly described in Algorithm 1. This approach effectively enhances student model’s performance by incrementally transferring valuable representations from long to short time steps.

Knowledge Distillation Method. For clarity, we will describe the knowledge distillation process within a single curriculum. It is straightforward to generalize this process to multiple curricula, since the same method is consistently applied in each curriculum setting. We denote $S(x)$ and $T(x)$ as the output logit vectors of the student and the teacher for input x , respectively. Formally, given a mini-batch, we first obtain the probability distribution $P_S(x; \tau)$ of the $S(x)$,

$$P_S(x; \tau) = \text{softmax}(S(x)/\tau), \quad (11)$$

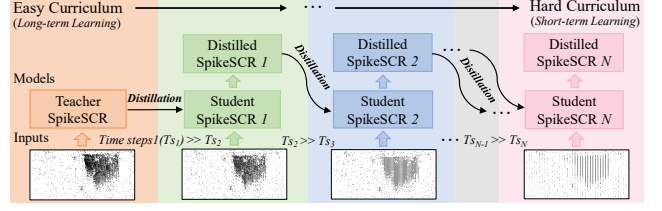


Figure 3: Illustration of our proposed KDCL. Taking the “yes” command from the SSC dataset as an example, the KDCL starts with an easy curriculum to learn the first teacher model, and then progressively distills student models under the next curriculum setting until the hardest curriculum is completed. This process gradually enhances the model’s performance from long time steps (long time sequences) to short time steps (short time sequences) through customized distillation across multiple curricula.

Algorithm 1: KDCL

Require:

Based on the easier curriculum: A trained teacher SNN model T_1 ; Training Dataset D_1 .

Based on the harder curriculum: A new student SNN model S_1 ; Training Dataset D_2 ;

Multi-Task Loss Function L_{MT} : Eq. (17).

Input: T_1, D_1, S_1, D_2 ; Total training iteration I_{train} ; Target class label Y .

Output: The well-trained SNN $S_1 \rightarrow$ The next curriculum level’s teacher model T_2 .

- 1: Frozen T_1 ; Init S_1 from T_1 ; D_1 and D_2 synchronization.
 - 2: **for** $i = 1$ to I_{train} **do**
 - 3: Get mini-batch data $x_1(i)$ from D_1 , mini-batch data $x_2(i)$ from D_2 , and class label $Y(i)$;
 - 4: Feed the $x_1(i)$ into the T_1 , feed the $x_2(i)$ into the S_1 ;
 - 5: Calculate the T_1 output $O_{T_1}(i)$ and the S_1 output $O_{S_1}(i)$;
 - 6: Compute loss $L_{MT} = \lambda_1 \mathcal{L}_{CE}(O_{S_1}(i), Y(i)) + \lambda_2 \mathcal{L}_{KD}(O_{T_1}(i), O_{S_1}(i))$;
 - 7: Calculate the derivative ∇L_{MT} of the loss;
 - 8: Update the S_1 weights $W = W - \eta \nabla L_{MT}$ where η is learning rate.
 - 9: **end for**
-

where τ denotes a temperature parameter (Kim et al. 2021). The probability distribution $P_T(x; \tau)$ of the $T(x)$ is computed in the same manner. Further, we focus on the Kullback-Leibler (KL) divergence between the two probability distributions (Wang, Cheng, and Lim 2022; Yang and Chen 2023). The divergence D_{KL} between $P_T(x; \tau)$ and $P_S(x; \tau)$ is computed for each instance as Eq. (12). Finally, the weighted loss L_{KD} is determined by averaging the D_{KL} across all M instances in the batch:

$$D_{KL}(P_T||P_S) = \sum_i P_{T_i} \log \left(\frac{P_{T_i}}{P_{S_i}} \right), \quad (12)$$

$$\mathcal{L}_{KD} = \frac{1}{M} \sum_{i=1}^M D_{KL}(P_T \parallel P_S). \quad (13)$$

Training Strategy

Note that the training of our model adopts the BPTT with surrogate gradients. We first introduce the input and output structure of SpikeSCR. Similar to the previous methods (Bitar and Garner 2022; Hammouamri, Khalfaoui-Hassani, and Masquelier 2024), the proposed models take inputs of size (B, T, N) , where B is the batch size, T is the number of time steps, and N is the number of input neurons or frequency bins. The number of classes is denoted by Y . The classification head outputs are each neuron’s synaptic potential through the time steps T . The method used to aggregate information from these time steps can be described as:

$$out_i[t] = \text{softmax}(s_i[t]) = \frac{e^{s_i[t]}}{\sum_{j=1}^Y e^{s_j[t]}}, \quad (14)$$

where $s_i[t] (t = 1, 2, \dots, T)$ is the synaptic potential of neuron i at time t . Then the final outputs of the model after T time steps return the size (B, C) , which can be defined as:

$$\hat{y}_i = \sum_{t=1}^T out_i[t]. \quad (15)$$

The cross-entropy loss L_{CE} for the classification task is calculated as Eq. (16). For the multi-task in a specified curriculum, the training objective L_{MT} is denoted as Eq. (17),

$$\mathcal{L}_{CE} = -\frac{1}{N} \sum_{n=1}^N \log(\text{softmax}(\hat{y}_n)[y_n]), \quad (16)$$

$$\mathcal{L}_{MT} = \lambda_1 \mathcal{L}_{CE} + \lambda_2 \mathcal{L}_{KD}, \quad (17)$$

where L_{KD} is detailed in Eq. (13). We set $\lambda_1 = 1.0$ and $\lambda_2 = 0.5$, which is refined through experiments, to balance the gradients in the overall learning process.

Experiments

Datasets and Experimental Setup

We evaluate our methods on two spiking datasets, SHD (Spiking Heidelberg Digits) and SSC (Spiking Speech Commands) (Cramer et al. 2020), and a non-spiking counterpart of SSC, GSC (Google Speech Commands V2) (Warden 2018). Both spiking datasets are constructed using artificial cochlear models to convert audio recording data to spikes. The SHD dataset consists of 10k recordings of 20 different classes, with spoken digits ranging from zero to nine in both English and German. SSC and GSC are much larger datasets, each containing 100k recordings. The task on SSC and GSC is the classification of all 35 different speech commands. We utilize the same preprocess methods (Hammouamri, Khalfaoui-Hassani, and Masquelier 2024) to all three datasets. For the two spiking datasets, the input neurons were reduced from 700 to 140 by using spatio-temporal bins across every 5 neurons. As for the temporal dimension,

we used a discrete time-step (which means at each Δt interval, the number of spikes is extracted) and a zero right-padding to ensure the same time duration (used as the time steps) of all recordings in one batch. For the GSC dataset, we used the Mel spectrogram of the waveforms with 140 frequency bins and approximately the same time steps consistent with the SSC. The dataset statistics and experimental setups are detailed in Appendix B. The empirical curriculum setting in KDCL is described as follows. For the SHD dataset, KDCL training involves two curricula from easy to hard: 100 time steps and 40 time steps, as the smaller dataset risks overfitting with excessive time steps. For the larger SSC and GSC datasets, KDCL involves four curricula from easy to hard: 500 (400), 200, 100, and 40 time steps.

Main Results

We compare our method to recent SNN works on the SHD (20 classes), SSC, and GSC (both with 35 classes) benchmark datasets in terms of accuracy and model size, as shown in Table 1. Even without knowledge transfer, our models surpass recent SOTA approaches across three benchmarks with the same time steps, including those focusing on learning delays in SNNs and modeling neuron dynamics. Notably, SpikeSCR achieves an accuracy of 82.54% on the SSC dataset with 100 time steps, demonstrating significant improvements compared to the current method DCLS (Hammouamri, Khalfaoui-Hassani, and Masquelier 2024), which achieves 80.69% accuracy with more parameters (2.5M vs. 1.63M). Moreover, the application of KDCL results in substantial improvements, achieving competitive results of 93.60%, 80.25%, and 95.01% on the SHD, SSC, and GSC datasets, respectively, with the fewest time steps (40) among compared works. Comprehensive results across all datasets are detailed in Appendix C due to space constraints.

We further validate our models’ capability for long-term learning over extended time steps, which is crucial for demonstrating the effectiveness of using a model with large time steps (such as 500 time steps) as the initial teacher model in subsequent KDCL procedures. As shown in Figure 4(a), we present the results of the SpikeSCR trained with either a single block or two blocks of SGL from scratch on the SSC dataset with various time steps: 40, 100, 200 and 500. We also compare our results with the reproduced DCLS method. The accuracy of SpikeSCR clearly improves as the number of time steps increases, rising from 79.23% to 85.57%. In contrast, DCLS shows optimal performance with 100 time steps but then declines with more time steps. This comparison indicates that SpikeSCR is better suited for long-term learning, effectively leveraging both comprehensive global contexts and detail-oriented local contexts. Figure 4(b) further illustrates the energy consumption results. As the number of time steps decreases, the energy consumption of SpikeSCR declines significantly. Specifically, from 100 to 40 time steps, the energy consumption for one block (blue) decreases by 53.8% (from 0.0171mJ to 0.0079mJ), and for two blocks (red), it decreases by 54.8% (from 0.0314mJ to 0.0142mJ). Notably, SpikeSCR demonstrates a significant energy efficiency advantage with 40 time steps, compared to the DCLS model.

Dataset	Model	Param (M)	Time Steps	Acc (%)
SHD	SpikeGRU (Dampfhoer et al. 2022)	—	250	87.80
	TC-LIF (Zhang et al. 2024b)	0.19	—	88.91
	Adaptive Axonal Delays (Sun et al. 2023b)	0.11	150	92.45
	DL256-SNN-Dloss (Sun et al. 2023a)	0.21	250	93.55
	SpikeSCR (1L-8-128)	0.25	40	93.60[†]/92.01
	RadLIF (Bittar and Garner 2022)	3.90	100	94.62
	DCLS-Delays (2L-1KC) (Hammouamri, Khalfaoui-Hassani, and Masquelier 2024)	0.20	100	95.07
	SpikeSCR (1L-8-128)	0.25	100	95.70
SSC	TC-LIF (Zhang et al. 2024b)	0.14	—	61.09
	SpikeGRU (Dampfhoer et al. 2022)	—	250	77.00
	RadLIF (Bittar and Garner 2022)	3.90	100	77.40
	DCLS-Delays (2L-2KC) (Hammouamri, Khalfaoui-Hassani, and Masquelier 2024)	1.40	100	80.16
	d-cAdLIF (Deckers et al. 2024)	0.70	100	80.23
	DCLS-Delays (3L-2KC) (Hammouamri, Khalfaoui-Hassani, and Masquelier 2024)	2.50	100	80.69
	SpikeSCR (1L-16-256)	1.63	40	79.76[†]/79.12
	SpikeSCR (1L-16-256)	1.63	100	82.99[†]/82.54
	SpikeSCR (2L-16-256)	3.15	40	80.25[†]/79.23
	SpikeSCR (2L-16-256)	3.15	100	83.69[†]/82.79
GSC	Speech2Spike (Stewart et al. 2023)	—	200	88.50
	TC-LIF (Zhang et al. 2024b)	0.61	—	88.91
	RadLIF (Bittar and Garner 2022)	1.20	100	94.51
	DCLS-Delays (2L-2KC) (Hammouamri, Khalfaoui-Hassani, and Masquelier 2024)	1.40	100	95.00
	Fully Spiking LMU Blocks (Liu et al. 2024b)	1.62	—	95.20
	DCLS-Delays (3L-2KC) (Hammouamri, Khalfaoui-Hassani, and Masquelier 2024)	2.50	100	95.35
	SpikeSCR (1L-16-256)	1.63	40	94.71[†]/94.50
	SpikeSCR (1L-16-256)	1.63	100	95.90[†]/95.56
	SpikeSCR (2L-16-256)	3.15	40	95.01[†]/94.54
	SpikeSCR (2L-16-256)	3.15	100	96.08[†]/95.60

Table 1: Comparison of model performances with prior SNN works on three different datasets, SHD, SSC and GSC. [†]indicates the performance after KDCL. The notation of (nL-m-d) in the table specifies the model architecture, where n represents the number of SGLE blocks, m represents the number of attention heads, and d represents the hidden size. For DCLS (nL-mKC), nL represents the number of layers and mKC is the number of kernel counts in dilated convolutions.

As in Figure 5, KDCL-based models demonstrate superior performance compared to those trained with the same number of time steps under the two blocks of SGLE. The models trained with KDCL consistently outperform those trained directly with any specified number of time steps. Notably, while models trained with large time steps (e.g., 500) achieve high performance, directly knowledge distillation from these teacher models to student models with merely 40 time steps yields marginal improvements (80.25% vs. 80.03%, 79.99%, and 79.67%). This suggests that excessively transferring knowledge from models with longer time steps to models with shorter time steps can be challenging in both performance and convergence. KDCL leads to the best results at 40 time steps, improving accuracy by 1.02% compared to direct training (80.25% vs. 79.23%). The comparable performance with SOTA methods like DCLS (2L-2KC) (80.25% vs. 80.16%; 40 steps vs. 100 steps) highlights its effectiveness with limited time steps.

Figure 6 illustrates the firing rate trends during the training process of the SN_2 neuron within the proposed SGU module across three datasets: SHD, SSC, and GSC. Over 300 training epochs with 100 time steps in a single block of SGLE, the firing rate initially increases and then stabilizes in the final 50 epochs, reaching approximately 30.6%

for SHD, 23.8% for SSC, and 16.9% for GSC. This stability and variability suggest that the SGU can adapt to different data patterns while efficiently maintaining gating mechanisms within the information flow and avoiding multiply-accumulate (MAC) operations (Chen et al. 2023), thereby validating the rationale and effectiveness of the design.

Table 2 presents the impact of different plug-and-play positional encodings on model performance and energy consumption. Compared to the model without PE, the sinusoidal positional encoding (SinPE) from the vanilla Transformer (Vaswani et al. 2017) improves performance by 1.24%. However, SinPE also increases energy consumption by nearly 5.2 times, as it transforms spike-form data into float-form data with positional information, thus increasing MAC operations. A LIF neuron layer integrated after applying SinPE could preserve the positional information in the spike sequences to keep low energy consumption, but only achieves 85.58% accuracy. In contrast, the integration of RoPE and LIF within the SSA maintains energy consumption levels comparable to those without positional encoding, while achieving the highest accuracy of 95.70%.

Comprehensive ablation studies are conducted with one SGLE block on the GSC dataset under 100 time steps, summarized in Table 3. Various components are systematically

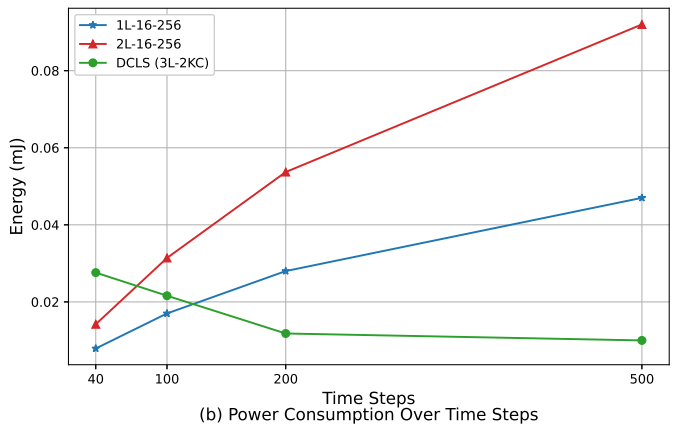
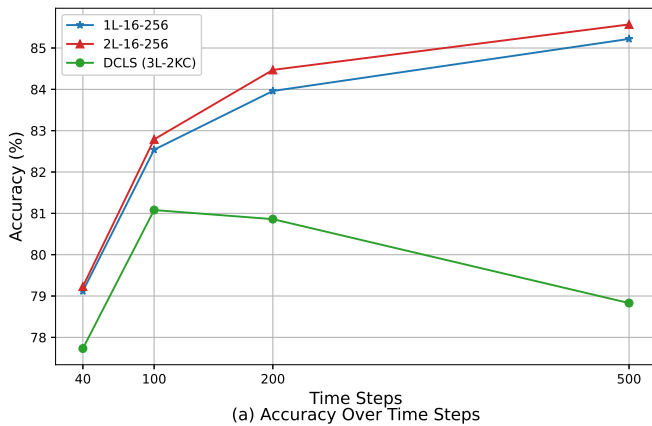


Figure 4: Comparative analysis of model performance and energy consumption from short to long time steps on SSC dataset.

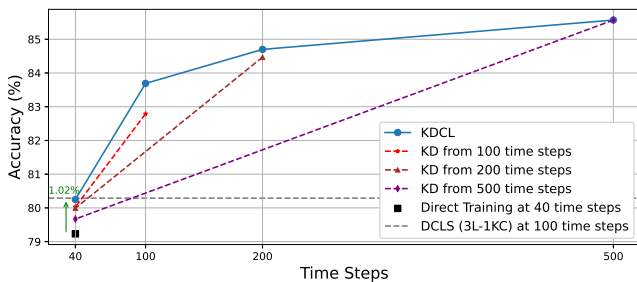


Figure 5: Comparing the performance of direct training, knowledge distillation, and KDCL on SSC dataset.

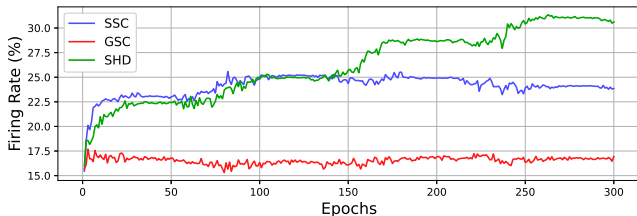


Figure 6: Firing rate of the LIF Neuron SN_2 in SGU on SHD, SSC and GSC datasets.

removed from the model, leading to performance reductions. The removal of the KDCL method results in a 0.34% decrease in accuracy. Further, eliminating the augment module reduces accuracy by an additional 0.57%. The impact of removing RoPE from the global representation learning module leads to a 0.34% reduction in accuracy. Omitting the spiking gated unit from the local representation learning module results in a 0.8% decrease. Moreover, the absence of the separable convolution module ($P_W + D_W + P_W$) causes a more significant decline, reducing accuracy by 1.08%.

Conclusion

In this study, we first propose a fully spike-driven framework, SpikeSCR, aiming at enhancing speech com-

Dataset	Position Encoding	Energy (mJ)	Acc (%)
SHD	None	0.005	93.69
	Sinusoidal PE (SinPE)	0.026	94.93
	SinPE + LIF	0.004	85.58
	RoPE + LIF	0.005	95.70

Table 2: The impact of different positional encodings on model performance and energy consumption.

Dataset	Model	Param (M)	Acc (%)
GSC	SpikeSCR (1L-16-256)	1.63	95.90
	w/o KDCL	1.63	95.56
	w/o SAM	1.63	94.99
	w/o RoPE	1.63	94.65
	w/o SGU	1.50	93.85
	w/o Separable Convolution	0.87	92.77

Table 3: Ablation studies on GSC dataset (100 time steps).

mand recognition. SpikeSCR effectively integrates position-embedded SSA and separable gated convolution to achieve global and local contextual representation learning. We demonstrate its efficient long-term learning capabilities, achieving excellent performance with extended time steps. To achieve a satisfactory trade-off between energy consumption and performance, we further introduce an effective knowledge distillation method, KDCL, where valuable representations learned from easy curriculum are progressively transferred to hard curriculum with minor loss. Our experimental results show that SpikeSCR outperforms SOTA methods across three benchmark datasets, achieving superior performance at the same time steps. Furthermore, through KDCL, SpikeSCR maintains comparable performance to SOTA results while reducing time steps by 60% and energy consumption by 54.8%.

References

- Bittar, A.; and Garner, P. N. 2022. A surrogate gradient spiking baseline for speech command recognition. *Frontiers in Neuroscience*, 16: 865897.
- Bu, T.; Fang, W.; Ding, J.; DAI, P.; Yu, Z.; and Huang, T. 2022. Optimal ANN-SNN Conversion for High-accuracy and Ultra-low-latency Spiking Neural Networks. In *International Conference on Learning Representations*.
- Chen, G.; Peng, P.; Li, G.; and Tian, Y. 2023. Training full spike neural networks via auxiliary accumulation pathway. *arXiv preprint arXiv:2301.11929*.
- Cramer, B.; Stradmann, Y.; Schemmel, J.; and Zenke, F. 2020. The heidelberg spiking data sets for the systematic evaluation of spiking neural networks. *IEEE Transactions on Neural Networks and Learning Systems*, 33(7): 2744–2757.
- Dampfhofer, M.; Mesquida, T.; Valentian, A.; and Anghel, L. 2022. Investigating current-based and gating approaches for accurate and energy-efficient spiking recurrent neural networks. In *International Conference on Artificial Neural Networks*, 359–370. Springer.
- Datta, G.; Kundu, S.; Jaiswal, A. R.; and Beerel, P. A. 2022. ACE-SNN: Algorithm-hardware co-design of energy-efficient & low-latency deep spiking neural networks for 3d image recognition. *Frontiers in Neuroscience*, 16: 815258.
- Dauphin, Y. N.; Fan, A.; Auli, M.; and Grangier, D. 2017. Language modeling with gated convolutional networks. In *International Conference on Machine Learning*, 933–941. PMLR.
- Deckers, L.; Van Damme, L.; Van Leekwijck, W.; Tsang, I. J.; and Latré, S. 2024. Co-learning synaptic delays, weights and adaptation in spiking neural networks. *Frontiers in Neuroscience*, 18: 1360300.
- Deng, S.; and Gu, S. 2021. Optimal Conversion of Conventional Artificial Neural Networks to Spiking Neural Networks. In *International Conference on Learning Representations*.
- Fang, W.; Chen, Y.; Ding, J.; Yu, Z.; Masquelier, T.; Chen, D.; Huang, L.; Zhou, H.; Li, G.; and Tian, Y. 2023. Spiking-jelly: An open-source machine learning infrastructure platform for spike-based intelligence. *Science Advances*, 9(40): eadi1480.
- Fang, W.; Yu, Z.; Chen, Y.; Huang, T.; Masquelier, T.; and Tian, Y. 2021. Deep Residual Learning in Spiking Neural Networks. In *Advances in Neural Information Processing Systems*, volume 34, 21056–21069.
- Gu, F.; Sng, W.; Hu, X.; and Yu, F. 2021. EventDrop: Data Augmentation for Event-based Learning. In *30th International Joint Conference on Artificial Intelligence, IJCAI 2021*.
- Gulati, A.; Qin, J.; Chiu, C.-C.; Parmar, N.; Zhang, Y.; Yu, J.; Han, W.; Wang, S.; Zhang, Z.; Wu, Y.; et al. 2020. Conformer: Convolution-augmented transformer for speech recognition. *arXiv preprint arXiv:2005.08100*.
- Guo, Y.; Chen, Y.; Liu, X.; Peng, W.; Zhang, Y.; Huang, X.; and Ma, Z. 2024. Ternary spike: Learning ternary spikes for spiking neural networks. In *Proceedings of the AAAI Conference on Artificial Intelligence*, volume 38, 12244–12252.
- Hammouamri, I.; Khalfaoui-Hassani, I.; and Masquelier, T. 2024. Learning Delays in Spiking Neural Networks using Dilated Convolutions with Learnable Spacings. In *International Conference on Learning Representations*.
- Horowitz, M. 2014. 1.1 computing’s energy problem (and what we can do about it). In *2014 IEEE international solid-state circuits conference digest of technical papers (ISSCC)*, 10–14. IEEE.
- Kim, K.; Ji, B.; Yoon, D.; and Hwang, S. 2021. Self-knowledge distillation with progressive refinement of targets. In *Proceedings of the IEEE/CVF International Conference on Computer Vision*, 6567–6576.
- Kim, Y.; Li, Y.; Park, H.; Venkatesha, Y.; Hambitzer, A.; and Panda, P. 2023. Exploring temporal information dynamics in spiking neural networks. In *Proceedings of the AAAI Conference on Artificial Intelligence*, volume 37, 8308–8316.
- Kugele, A.; Pfeil, T.; Pfeiffer, M.; and Chicca, E. 2020. Efficient processing of spatio-temporal data streams with spiking neural networks. *Frontiers in Neuroscience*, 14: 512192.
- Lee, C.; Sarwar, S. S.; Panda, P.; Srinivasan, G.; and Roy, K. 2020. Enabling spike-based backpropagation for training deep neural network architectures. *Frontiers in Neuroscience*, 14: 497482.
- Lee, J. H.; Delbruck, T.; and Pfeiffer, M. 2016. Training deep spiking neural networks using backpropagation. *Frontiers in Neuroscience*, 10: 508.
- Liu, F.; Wang, Z.; Zhao, W.; Yang, N.; Chen, Y.; Huang, S.; Li, H.; Yang, T.; Pei, S.; Liang, X.; et al. 2024a. Exploiting Temporal-Unrolled Parallelism for Energy-Efficient SNN Acceleration. *IEEE Transactions on Parallel & Distributed Systems*, (01): 1–16.
- Liu, Z.; Datta, G.; Li, A.; and Beerel, P. A. 2024b. LMU-Former: Low Complexity Yet Powerful Spiking Model With Legendre Memory Units. In *International Conference on Learning Representations*.
- Logan, B.; et al. 2000. Mel frequency cepstral coefficients for music modeling. In *Ismir*, volume 270, 11.
- Maass, W. 1997. Networks of spiking neurons: the third generation of neural network models. *Neural Networks*, 10(9): 1659–1671.
- Neftci, E. O.; Mostafa, H.; and Zenke, F. 2019. Surrogate gradient learning in spiking neural networks: Bringing the power of gradient-based optimization to spiking neural networks. *IEEE Signal Processing Magazine*, 36(6): 51–63.
- Panda, P.; Aketi, S. A.; and Roy, K. 2020. Toward scalable, efficient, and accurate deep spiking neural networks with backward residual connections, stochastic softmax, and hybridization. *Frontiers in Neuroscience*, 14: 653.
- Park, D. S.; Chan, W.; Zhang, Y.; Chiu, C.-C.; Zoph, B.; Cubuk, E. D.; and Le, Q. V. 2019. SpecAugment: A simple data augmentation method for automatic speech recognition. *arXiv preprint arXiv:1904.08779*.
- Rathi, N.; Chakraborty, I.; Kosta, A.; Sengupta, A.; Ankit, A.; Panda, P.; and Roy, K. 2023. Exploring neuromorphic computing based on spiking neural networks: Algorithms to hardware. *ACM Computing Surveys*, 55(12): 1–49.

- Rathi, N.; and Roy, K. 2021. Diet-snn: A low-latency spiking neural network with direct input encoding and leakage and threshold optimization. *IEEE Transactions on Neural Networks and Learning Systems*, 34(6): 3174–3182.
- Roy, K.; Jaiswal, A. R.; and Panda, P. 2019. Towards spike-based machine intelligence with neuromorphic computing. *Nature*, 575: 607 – 617.
- Sengupta, A.; Ye, Y.; Wang, R.; Liu, C.; and Roy, K. 2019. Going deeper in spiking neural networks: VGG and residual architectures. *Frontiers in Neuroscience*, 13: 95.
- Shen, J.; Pang, R.; Weiss, R. J.; Schuster, M.; Jaitly, N.; Yang, Z.; Chen, Z.; Zhang, Y.; Wang, Y.; Skerrv-Ryan, R.; et al. 2018. Natural tts synthesis by conditioning wavenet on mel spectrogram predictions. In *2018 IEEE International Conference on Acoustics, Speech and Signal Processing (ICASSP)*, 4779–4783. IEEE.
- Shen, S.; Zhao, D.; Shen, G.; and Zeng, Y. 2024. TIM: An Efficient Temporal Interaction Module for Spiking Transformer. *arXiv preprint arXiv:2401.11687*.
- Stewart, K. M.; Shea, T.; Pacik-Nelson, N.; Gallo, E.; and Danielescu, A. 2023. Speech2spikes: Efficient audio encoding pipeline for real-time neuromorphic systems. In *Proceedings of the 2023 Annual Neuro-Inspired Computational Elements Conference*, 71–78.
- Su, J.; Ahmed, M.; Lu, Y.; Pan, S.; Bo, W.; and Liu, Y. 2024. Roformer: Enhanced transformer with rotary position embedding. *Neurocomputing*, 568: 127063.
- Su, Q.; Chou, Y.; Hu, Y.; Li, J.; Mei, S.; Zhang, Z.; and Li, G. 2023. Deep directly-trained spiking neural networks for object detection. In *Proceedings of the IEEE/CVF International Conference on Computer Vision*, 6555–6565.
- Sun, P.; Chua, Y.; Devos, P.; and Botteldooren, D. 2023a. Learnable axonal delay in spiking neural networks improves spoken word recognition. *Frontiers in Neuroscience*, 17: 1275944.
- Sun, P.; Eqlimi, E.; Chua, Y.; Devos, P.; and Botteldooren, D. 2023b. Adaptive Axonal Delays in Feedforward Spiking Neural Networks for Accurate Spoken Word Recognition. In *2023 IEEE International Conference on Acoustics, Speech and Signal Processing (ICASSP)*, 1–5.
- Vaswani, A.; Shazeer, N.; Parmar, N.; Uszkoreit, J.; Jones, L.; Gomez, A. N.; Kaiser, Ł.; and Polosukhin, I. 2017. Attention is all you need. *Advances in Neural Information Processing Systems*, 30.
- Wang, S.; Cheng, T. H.; and Lim, M.-H. 2022. LTMD: learning improvement of spiking neural networks with learnable thresholding neurons and moderate dropout. *Advances in Neural Information Processing Systems*, 35: 28350–28362.
- Warden, P. 2018. Speech commands: A dataset for limited-vocabulary speech recognition. *arXiv preprint arXiv:1804.03209*.
- Wu, X.; Zhao, Y.; Song, Y.; Jiang, Y.; Bai, Y.; Li, X.; Zhou, Y.; Yang, X.; and Hao, Q. 2023. Dynamic threshold integrate and fire neuron model for low latency spiking neural networks. *Neurocomputing*, 544: 126247.
- Xu, M.; Chen, X.; Guo, Y.; Wang, Y.; Qiu, D.; Du, X.; Cui, Y.; Wang, X.; and Xiong, J. 2023a. Reconfigurable neuromorphic computing: Materials, devices, and integration. *Advanced Materials*, 35(51): 2301063.
- Xu, Q.; Li, Y.; Shen, J.; Liu, J. K.; Tang, H.; and Pan, G. 2023b. Constructing deep spiking neural networks from artificial neural networks with knowledge distillation. In *Proceedings of the IEEE/CVF Conference on Computer Vision and Pattern Recognition*, 7886–7895.
- Yang, H.; Lam, K.-Y.; Xiao, L.; Xiong, Z.; Hu, H.; Niyato, D.; and Vincent Poor, H. 2022. Lead federated neuromorphic learning for wireless edge artificial intelligence. *Nature Communications*, 13(1): 4269.
- Yang, Q.; Liu, Q.; and Li, H. 2022. Deep residual spiking neural network for keyword spotting in low-resource settings. In *Interspeech*, 3023–3027.
- Yang, S.; and Chen, B. 2023. SNIB: improving spike-based machine learning using nonlinear information bottleneck. *IEEE Transactions on Systems, Man, and Cybernetics: Systems*, 53(12): 7852–7863.
- Yao, M.; Gao, H.; Zhao, G.; Wang, D.; Lin, Y.; Yang, Z.; and Li, G. 2021. Temporal-wise attention spiking neural networks for event streams classification. In *Proceedings of the IEEE/CVF International Conference on Computer Vision*, 10221–10230.
- Yao, M.; Hu, J.; Hu, T.; Xu, Y.; Zhou, Z.; Tian, Y.; XU, B.; and Li, G. 2024. Spike-driven Transformer V2: Meta Spiking Neural Network Architecture Inspiring the Design of Next-generation Neuromorphic Chips. In *International Conference on Learning Representations*.
- Zhang, H.; Zhou, C.; Yu, L.; Huang, L.; Ma, Z.; Fan, X.; Zhou, H.; and Tian, Y. 2024a. SGLFormer: Spiking Global-Local-Fusion Transformer with High Performance. *Frontiers in Neuroscience*, 18: 1371290.
- Zhang, S.; Yang, Q.; Ma, C.; Wu, J.; Li, H.; and Tan, K. C. 2024b. Tc-lif: A two-compartment spiking neuron model for long-term sequential modelling. In *Proceedings of the AAAI Conference on Artificial Intelligence*, volume 38, 16838–16847.
- Zhou, C.; Zhang, H.; Yu, L.; Ye, Y.; Zhou, Z.; Huang, L.; Ma, Z.; Fan, X.; Zhou, H.; and Tian, Y. 2024. Direct training high-performance deep spiking neural networks: a review of theories and methods. *Frontiers in Neuroscience*, 18.
- Zhou, Z.; Zhu, Y.; He, C.; Wang, Y.; YAN, S.; Tian, Y.; and Yuan, L. 2023. Spikformer: When Spiking Neural Network Meets Transformer. In *International Conference on Learning Representations*.
- Zhu, R.-J.; Zhang, M.; Zhao, Q.; Deng, H.; Duan, Y.; and Deng, L.-J. 2024. Tcja-snn: Temporal-channel joint attention for spiking neural networks. *IEEE Transactions on Neural Networks and Learning Systems*, 1–14.

Appendix

Appendix A: Augments

We utilize SpecAugment (Park et al. 2019) with frequency masking and time masking for the Mel spectrogram of the input audio. The specific parameter settings for SpecAugment are detailed in Table 4. Additionally, we present a comparison of the augmented data in Figure 7, illustrating a "Right" command sample before and after data augmentation. For the spike trains in SHD and SSC, we utilize a method similar to EventDrop (Gu et al. 2021) involves two operations: drop-by-time and drop-by-neuron, both performed at a fixed ratio to drop events in different dimensions randomly. The specific parameter settings for EventDrop are detailed in Table 4. We also present a comparison of the augmented data in Figure 8, illustrating a "Cat" command sample before and after data augmentation.

Parameter	GSC
Number of Frequency Masks	1
Frequency Mask Size	10
Number of Time Masks	1
Time Mask Size	0.25
Parameter	SHD / SSC
Drop Proportion	0.5 / 0.5
Time Drop Size	0.2 / 0.1
Neuron Drop Size	20 / 10

Table 4: Augmentation parameters for three datasets.

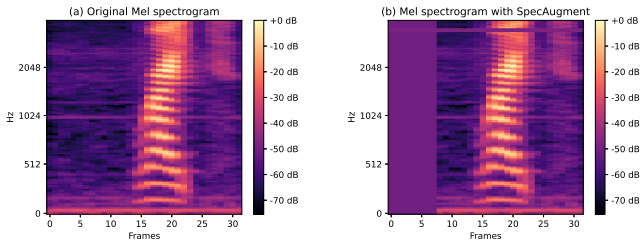


Figure 7: Comparison of the "Right" command in GSC dataset before and after augmentation.

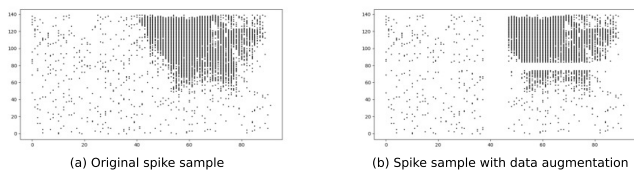


Figure 8: Comparison of the "Cat" command in SSC dataset before and after augmentation.

Appendix B: Datasets and Experimental Setup

The dataset statistics of three benchmark datasets are shown in Table 5. The SHD dataset consists of recordings of spoken

digits ranging from zero to nine in English and German language. There are only training and testing sets, with a total of 10,420 samples in SHD dataset. SSC is the spiking version of GSC. Both SSC and GSC have the same total number of samples, 105,829, which consist of a total of 35 word commands (Yes, No, Up, Down, Left, Right, etc), although the number of training and testing samples differ slightly. Overall, the number of samples of SSC and GSC are nearly ten times that of SHD. Therefore, we set two learning curricula for SHD and four learning curricula for SSC and GSC. Our work is implemented using the PyTorch-based Spiking-Jelly (Fang et al. 2023) framework. Additionally, we provide detailed experimental settings for the three datasets, as shown in Table 6. It is worth noting that to ensure the stability of the knowledge distillation process, we further employ a warming-up strategy, setting it for the initial 10 epochs.

Datasets	Training Sample	Validation Sample	Testing Sample
SHD	8156	—	2264
SSC	75466	9981	20382
GSC	84843	9981	11005

Table 5: Dataset statistics of three datasets.

Appendix C: Comprehensive Results

To provide a more comprehensive understanding of the impact of our SpikeSCR framework and KDCL method across different datasets, we present detailed evaluations in this section, which can showcase the robust adaptability of our proposed framework and method.

Figure 4 presents a comparative analysis of model performance and energy consumption from short to long time steps on the SSC dataset. We further provide detailed numerical statistics in terms of time steps, parameters, energy and accuracy, showcasing in Table 7, and conduct a thorough analysis. Across all time steps, SpikeSCR outperforms the DCLS model, where (3L-2KC) represents a 3-layer feed-forward network with dilated convolutions and 2 learnable kernel counts used for learning synaptic delays. With 40 time steps, SpikeSCR exhibits lower energy consumption

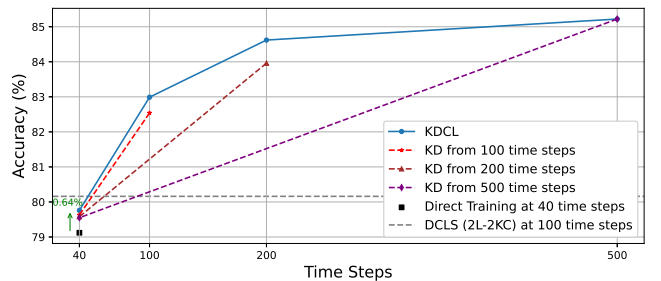


Figure 9: Comparing the performance of SpikeSCR with a single block of SGLE among direct training, knowledge distillation, and KDCL on SSC dataset.

Datasets	SHD	SSC	GSC
Direct Training Epochs	300	300	300
Knowledge Distillation Epochs	300	400	400
Batch Size		256	
Optimizer		AdamW	
Weight Decay	1e-2	1e-2	5e-3
Surrogate Function		Atan ($\alpha=5.0$)	
Learning Rate	1e-2	5e-3	2e-3
LR Scheduler		Cosine Annealing, $T_{\max}=40$	
Spiking Neuron		LIF ($\tau=2.0, V_{\text{threshold}}=1.0$)	
GPU		RTX 4090	

Table 6: Implementation details for SHD, SSC, and GSC datasets.

Dataset	Model	Time Steps	Param (M)	Energy (mJ)	Acc (%)
SSC	DCLS-Delays (3L-2KC)	40	2.34	0.0276	77.73
	SpikeSCR (1L-16-256)	40	1.63	0.0079	79.12
	SpikeSCR (2L-16-256)	40	3.15	0.0142	79.23
	DCLS-Delays (3L-2KC)	100	2.34	0.0216	81.08
	SpikeSCR (1L-16-256)	100	1.63	0.0171	82.54
	SpikeSCR (2L-16-256)	100	3.15	0.0314	82.79
	DCLS-Delays (3L-2KC)	200	2.34	0.0118	80.86
	SpikeSCR (1L-16-256)	200	1.63	0.0270	83.96
	SpikeSCR (2L-16-256)	200	3.15	0.0537	84.47
	DCLS-Delays (3L-2KC)	500	2.34	0.0110	78.76
	SpikeSCR (1L-16-256)	500	1.63	0.0472	85.22
	SpikeSCR (2L-16-256)	500	3.15	0.0920	85.57

Table 7: Quantitative comparison of performance and energy consumption between SpikeSCR and DCLS across various time steps on SSC dataset.

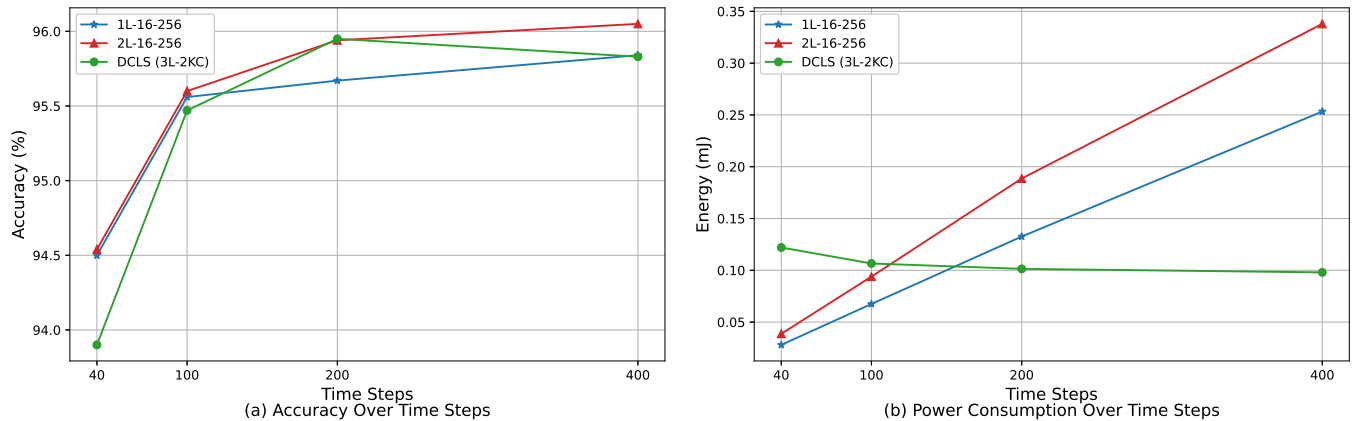


Figure 10: Comparative analysis of performance and energy consumption from short to long time steps on GSC dataset.

than DCLS (0.0079mJ and 0.0142mJ vs. 0.0276mJ). With 100 time steps, the energy consumption of SpikeSCR begins to show an increasing trend. Specifically, SpikeSCR with one SGLE block still exhibits competitive energy consumption (0.0171 mJ vs. 0.0216 mJ). However, with two SGLE blocks, its energy consumption surpasses that of DCLS

(0.0314 mJ vs. 0.0216 mJ). Moreover, at 200, and 500 time steps, SpikeSCR’s energy consumption gradually increases. Although DCLS mitigates rising energy consumption by learning delays with only a few kernel counts, its performance deteriorates with increasing time steps (from 77.77%, 81.08%, 80.86% to 78.76%), indicating a lack of long-term

Dataset	Model	Time Steps	Param (M)	Energy (mJ)	Acc (%)
GSC	DCLS-Delays (3L-2KC)	40	2.34	0.1220	93.90
	SpikeSCR (1L-16-256)	40	1.63	0.0280	94.50
	SpikeSCR (2L-16-256)	40	3.15	0.0387	94.54
	DCLS-Delays (3L-2KC)	100	2.34	0.1066	95.47
	SpikeSCR (1L-16-256)	100	1.63	0.0675	95.56
	SpikeSCR (2L-16-256)	100	3.15	0.0939	95.60
	DCLS-Delays (3L-2KC)	200	2.34	0.1014	95.95
	SpikeSCR (1L-16-256)	200	1.63	0.1326	95.67
	SpikeSCR (2L-16-256)	200	3.15	0.1886	95.94
	DCLS-Delays (3L-2KC)	400	2.34	0.0980	95.83
	SpikeSCR (1L-16-256)	400	1.63	0.2533	95.84
	SpikeSCR (2L-16-256)	400	3.15	0.3379	96.05

Table 8: Quantitative comparison of performance and energy consumption between SpikeSCR and DCLS across various time steps on GSC dataset.

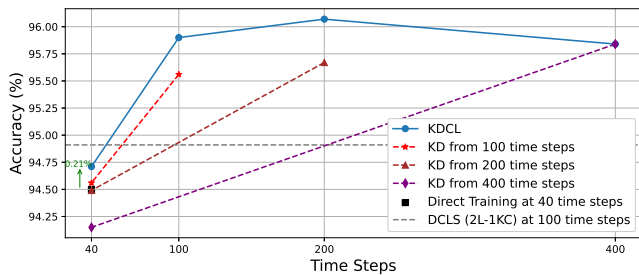


Figure 11: Comparing the performance of SpikeSCR with a single block of SGLE among direct training, knowledge distillation, and KDCL on GSC dataset.

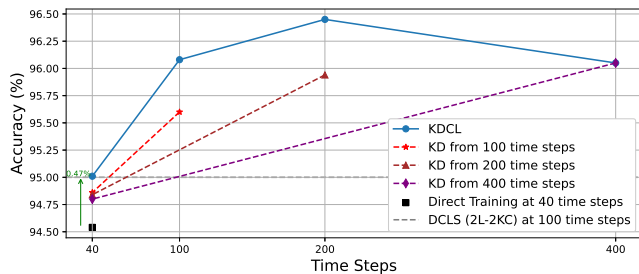


Figure 12: Comparing the performance of SpikeSCR with two blocks of SGLE among direct training, knowledge distillation, and KDCL on GSC dataset.

learning capability. Additionally, we further demonstrate the superior performance of KDCL-based models compared to those trained with the same time steps under only one block of SGLE, as shown in Figure 9. Consistent with the conclusions from Figure 5, KDCL-based models consistently outperform those trained directly at any specified time step. Direct knowledge distillation from these teacher models with large time steps to student models with only 40 time steps yields inconspicuous outcomes (79.76% vs. 79.63%,

79.58%, and 79.55%). KDCL achieves the most promising results at 40 time steps, improving accuracy by 0.64% compared to direct training (79.76% vs. 79.12%). The comparable performance with SOTA methods like DCLS (2L-2KC) (79.76% vs. 80.16%; 40 steps vs. 100 steps) highlights KDCL’s effectiveness with limited time steps.

Figure 10 presents a comparative analysis of model performance and energy consumption across different time steps on the GSC dataset, with detailed numerical statistics provided in Table 8. In terms of performance, SpikeSCR continues to demonstrate long-term learning capabilities as the number of time steps increases, showing a consistent upward trend. In contrast, DCLS achieves its best results at 200 time steps but shows a noticeable decline at 400 time steps. For Mel spectrogram inputs, SpikeSCR exhibits greater advantages in energy consumption compared to DCLS. At 40 and 100 time steps, the energy consumption for both one and two SGLE blocks are lower than that of DCLS. Specifically, at 40 time steps, energy consumption is 0.0280 mJ and 0.0384 mJ for one and two SGLE blocks respectively, compared to DCLS’s 0.1220 mJ. With 100 time steps, energy consumption is 0.0675 mJ and 0.0939 mJ for SpikeSCR, compared to DCLS’s 0.1066 mJ. However, there is a clear upward trend in SpikeSCR’s energy consumption at 200 and 400 time steps.

Furthermore, we demonstrate the superior performance of KDCL-based models compared to those trained under the same time steps using one block and two blocks of SGLE on the GSC dataset, as illustrated in Figure 11 and Figure 12. Consistent with the conclusions on the SSC dataset, KDCL-based models outperform those trained directly at any specified time step. Direct knowledge distillation from these teacher models with large time steps to student models with only 40 time steps yields inconspicuous outcomes. For one block of SGLE, it achieves 94.71% compared to 94.56%, 94.49% and 94.15%. KDCL achieves the most promising results at 40 time steps, improving accuracy by 0.21% compared to direct training (94.71% vs. 94.50%). The comparable performance with DCLS (2L-1KC) (94.71% vs. 94.91%;

Dataset	Position Encoding	Energy (mJ)	Acc (%)
SSC	None	0.0173	81.79
	Sinusoidal PE (SinPE)	0.0609	81.59
	SinPE + LIF	0.0145	66.48
	RoPE + LIF	0.0169	81.94

Table 9: Different positional encodings on SSC dataset.

Dataset	Model	Param (M)	Acc (%)
SHD	SpikeSCR (1L-8-128)	0.25	95.70
	w/o SAM	0.25	94.55
	w/o RoPE	0.25	93.69
	w/o SGU	0.22	92.93
	w/o Separable Convolution	0.15	88.36

Table 10: Ablation studies on SHD dataset (100 time steps).

40 steps vs. 100 steps) highlights its effectiveness with limited time steps. For two blocks of SGLE, it achieves 95.01% compared to 94.86%, 94.84%, and 94.80%. KDCL achieves the most promising results at 40 time steps, improving accuracy by 0.47% compared to direct training (95.01% vs. 94.54%). The comparable performance with SOTA methods like DCLS (2L-2KC) (95.01% vs. 95.00%; 40 steps vs. 100 steps) demonstrates KDCL’s efficiency when operating with fewer time steps.

We further discuss the impact of different plug-and-play positional encodings on model performance and energy consumption on the larger-scale SSC dataset, as detailed in Table 9. Compared to the baseline without PE, which achieves an accuracy of 81.79% and energy consumption of 0.0173 mJ, the SinPE slightly decreases performance to 81.59% while increasing energy consumption to 0.0609 mJ, about 3.5 times higher, due to the transformation of spike-form data into float-form data. Integrating SinPE with a LIF neuron significantly reduces energy consumption to 0.0145 mJ, but at the cost of dramatically decreasing accuracy to 66.48%. In contrast, the integration of RoPE with LIF maintains energy consumption at 0.0169 mJ, comparable to the baseline without PE, and achieves the highest accuracy of 81.94% among the tested encodings.

Comprehensive ablation studies are conducted on the smaller-scale, spike-form SHD dataset with 100 time steps, with results summarized in Table 10. Eliminating the augment module reduces accuracy by an additional 1.15%. The impact of removing RoPE from the global representation learning module lead to a 0.86% reduction in accuracy. Omitting the spiking gated unit from the local representation learning module results in a 0.76% decrease. Moreover, the absence of the separable convolution module causes a more significant decline, reducing 4.57%.

Appendix D: Theoretical Calculation of Energy Consumption

The theoretical energy consumption of an SNN is usually calculated through multiplication between the number of

MAC/AC operations and the energy consumption of each operation on predefined hardware (Panda, Aketi, and Roy 2020; Zhou et al. 2023; Yao et al. 2024; Zhang et al. 2024a). The number of synaptic operations (SOPs) is calculated as:

$$SOP^l = fr^{l-1} \times FLOP^l, \quad (18)$$

where fr^{l-1} is the firing rate of spiking neuron layer $l - 1$. $FLOP^l$ refers to the number of floating-point MAC operations (FLOPs) of layer l , and SOP^l is the number of spike-based AC operations (SOPs). Assuming the MAC and AC operations are performed on the 45nm hardware (Horowitz 2014), i.e. $E_{MAC} = 4.6pJ$ and $E_{AC} = 0.9pJ$, the energy consumption of SpikeSCR can be calculated as follows:

$$E = E_{AC} \times \left(\sum_{i=1}^N SOP_{Conv}^i + \sum_{j=1}^M SOP_{SSA}^j \right), \quad (19)$$

$$E = E_{MAC} \times (FLOP_{Conv}^1) + E_{AC} \times \left(\sum_{i=2}^N SOP_{Conv}^i + \sum_{j=1}^M SOP_{SSA}^j \right) \quad (20)$$

SOP_{Conv} represents the SOPs of a convolution or linear layer, and SOP_{SSA} represents the SOPs of an SSA module, $FLOP_{Conv}^1$ represents the FLOPs of the first layer before encoding input frames into spikes. N is the total number of convolution layers and linear layers, and M is the number of SSA modules. During model inference, several cascaded linear operation layers such as convolution, linear, and BN layers, can be fused into one single linear operation layer (Zhou et al. 2024), still enjoying the AC-type operations with a spike-form input tensor.

We further explain the energy consumption calculation under two different input conditions. Specifically, when the input to SpikeSCR is in spike-form (such as the SHD and SSC datasets), it does not involve MAC operations, and thus its energy consumption is calculated as shown in Eq. 19. However, when the input to SpikeSCR is in real-valued form (such as the GSC dataset), the first Conv layer in the SEM involves MAC operations, and its energy consumption is calculated as shown in Eq. 20.

Appendix E: Code Available

We utilize the SpikingJelly framework (Fang et al. 2023) to train our model, available at <https://github.com/fangwei123456/spikingjelly>.

For comparison, we select the currently reproducible SOTA work DCLS (Hammouamri, Khalfaoui-Hassani, and Masquelier 2024), with code available at <https://github.com/Thvntos/SNN-delays>. Moreover, we employ the same data preprocessing methods as those used in the DCLS work to ensure consistency in our experimental setup.

Our energy consumption calculation framework is based on syops-counter (Chen et al. 2023), with code available at <https://github.com/iCGY96/syops-counter>.

Our organized code will be made publicly available on a common repository upon reaching the camera-ready version of this paper.